Freezing Behavior in Porous Materials: Theory and Experiment[*]

by M. Sliwinska-Bartkowiak[1], G. Dudziak[1], R. Sikorski[1], R. Gras[1], K.E. Gubbins[2], R. Radhakrishnan[2**] and K. Kaneko[3]

[1]*Institute of Physics, University of A. Mickiewicz, Umultowska 85, 61-614 Poznan, Poland*
[2]*North Carolina State University,113 Riddick Labs, Raleigh, NC 27695-7905, USA*
[3]*Department of Chemistry, Faculty of Science, Chiba University, Yayoi 1-33, Inage, Chiba 263-8522, Japan*

We report both experimental measurements and molecular simulations of the melting and freezing behavior of simple fluids in porous media. Activated carbon fibers, having a mean pore width of 1.7 nm, were chosen as the porous medium. Differential scanning calorimetry (DSC) and dielectric relaxation spectroscopy (DS) were used to determine the melting point in these materials. The melting point was found to be very sensitive to the relative strength of the fluid-wall interaction compared to the fluid-fluid interaction. Monte Carlo simulations and Landau free energy formalism were used to determine the shift in the melting point, T_m, for simple fluids in pores having repulsive, weakly attractive and strongly attractive walls. The strength of the interaction of the fluid with the pore wall is shown to have a large effect on the shift in T_m, with T_m being reduced for weakly attracting walls. The theory of corresponding states is used to compare the experimental results for several systems to the simulation results. This approach also provides a unified approach in understanding the diverse freezing behavior in porous media.

Key words: simulation, phase transition, calorimetry, corresponding states, fluids, porous media, hysteresis

Recently, there has been growing interest in the study of fluid-solid transitions in porous materials. Important questions are the nature of the phase transition (first order *vs*. continuous), the direction of shift in the melting temperature T_m, nature and origin of hysteresis, dimensionality cross-over due to increasing confinement, structural changes of the condensed phases in the restricted pore geometries, effect on latent heats, *etc*. Improved understanding of confinement effects on freezing are essential in areas relating to lubrication, adhesion, fabrication of nanomaterials and nanotribology. In addition, these studies can provide insight into mechanisms involved in frost heaving and distribution of pollutants in soil. Freezing in porous media has also been widely employed in the characterization of porous materials using the method of

---

thermoporometry. Some other possible applications are in the development of novel materials for energy storage, high-speed vehicles and aircraft braking systems [1,2].

Experiments on melting that have used porous silica glass as the confinement medium have always resulted in a decrease in the melting temperature, T_m, as compared to the bulk. Melting of oxygen in sol-gel glasses was studied by Warnock *et. al.* [3] by a sub-pico second optical technique. In this method, birefringence in optical pump pulses caused by the rotational motion of the molecules in the liquid was used to measure the subsequent molecular orientational relaxation time. A change in the value of the relaxation time provided an indication of the freezing temperature. The melting temperature in the confined system was always depressed as compared to the bulk; the shift was larger for smaller pores and as large as 10 K for the smallest (20 nm) pore. Unruh and co-workers [4] examined the melting behavior of indium metal in porous silica glasses by differential scanning calorimetry (DSC) measurements and reported a large depression in melting point due to confinement. In view of the large body of experimental evidence for a decrease in the melting temperature due to confinement ([5] and the refs. therein), it is tempting to assume that a decrease always occurs. However, a classical thermodynamic argument based on simple capillary theory determines the melting temperature as the point at which the chemical potential of the solid core inside the pore equals that of the surrounding fluid (for example, see [5]),

$$\frac{\Delta T_m}{T_{mb}} = -2\frac{(\gamma_{ws} - \gamma_{wl})\nu}{H\lambda_{mb}} \tag{1}$$

where T_{mb} is the bulk melting temperature, γ_{ws} and γ_{wl} are the corresponding wall-solid and wall-fluid surface tensions, ν is the molar volume of the liquid, λ_{mb} is the latent heat of melting in the bulk and H is the pore width. Equation (1) is sometimes referred to as the Gibbs-Thomson equation and predicts that the sign of $\Delta T_m = T_m - T_{mb}$ depends on whether γ_{ws} is greater or less than γ_{wl}. In a subsequent molecular simulation study of the effect of confinement on freezing of simple fluids in slit pores by Miyahara and Gubbins [6], it was shown that T_m was strongly affected by the strength of the attractive forces between the fluid molecules and the pore walls. For repulsive or weakly attractive potentials, the shift in the freezing temperature ΔT_m was negative. For strongly attracting walls such as carbons, an *increase* in T_m was observed. Thus, Miyahara and Gubbins explained the disparate experimental trends on the direction of the shift in the freezing temperature and provided the connection to the Gibbs-Thomson equation. The predictions of Miyahara and Gubbins were confirmed by free energy studies that provided the thermodynamic freezing temperature in confined systems; these studies established that the freezing transition remained first order despite the varied dimensionality [7,8].

The first experimental evidence of an elevation in freezing temperature for confined systems was reported by Klein and Kumacheva [9]. These authors studied

freezing of cyclohexane between parallel mica surfaces (slit shaped geometry) and observed a significant *increase* of about 17 K in the melting temperature on confinement (in a 4.0 nm pore). Similar phenomenon has been observed for linear alkanes confined between mica surfaces [10,11]. More recently, Castro *et. al*. [12] studied freezing of methane and other liquid alkanes on a graphite substrate by incoherent elastic neutron scattering. They found that the layer nearest to the graphite substrate melts at a temperature 10% higher than the bulk melting point of methane. The elevation in the freezing temperature in confined systems remain controversial, as there have been contradicting reports on the nature of the shift in the freezing temperature of cyclohexane between parallel mica surfaces in a surface force apparatus [13].

In this paper, we report a systematic study of the effect of the strength of the pore wall interaction on the freezing/melting behavior of confined fluids. The DSC and dielectric spectroscopy experiments were performed at Adam Mickiewicz University, Poznan, Poland, and Chiba University, Chiba, Japan; the molecular simulations were performed at North Carolina State University, USA.

EXPERIMENTAL

Differential Scanning Calorimetry. Four different fluids, *viz*., nitrobenzene, aniline, benzene and water, were chosen for study. Activated carbon fibers (ACF's) were chosen as the confinement medium. This material had slit-shaped pores of mean width H = 1.7 nm, and a narrow pore size distribution. Perkin-Elmer DSC-7 and Dupont thermal analyzers were used to determine the melting temperatures and latent heats of fusion, by measuring the heat released in the melting of the bulk fluid and confined fluid. Temperature scanning rates of 0.5–2 K/min were used in the experiments. The melting temperatures were determined from the position of the peaks of the heat flow signals and the latent heats were determined based on the scaled area under these signals. The melting temperatures were reproducible to within 0.5°C for larger pores ($\geq$ 25 nm); uncertainties were larger for the smaller pores. The latent heats were reproducible to within an accuracy of 5%.

Dielectric relaxation spectroscopy. The relative permittivity of a medium, $\kappa^* = \kappa' - i\kappa''$, is in general a complex quantity, whose real part κ' (also known as the dielectric constant) is associated with the increase in capacitance, due to the introduction of the dielectric. The imaginary component κ'' is associated with mechanisms that contribute to energy dissipation in the system, due to viscous damping of the rotational motion of the dipolar molecules in alternating fields. The latter effect is frequency dependent. The experimental setup consisted of a parallel plate capacitor of empty capacitance $C_0 = 42$ pF. The capacitance, C, and the tangent loss, $\tan(\delta)$, of the capacitor filled with nitrobenzene between the plates were measured using a Solartron 1260 Gain Impedance analyzer, in the frequency range 1 Hz – 10 MHz, for various temperatures. For the case of nitrobenzene in porous silica, the sample was introduced between the capacitor plates as a suspension of 200 μm mesh porous silica particles in pure nitrobenzene. For the case of suspensions with large conductivity, the electrodes were blocked using a teflon film. The contributions to κ^* were determined from,

$$\kappa' = \frac{C}{C_0}; \quad \kappa'' = \frac{\tan(\delta)}{\kappa'} \tag{2}$$

In equation (2), C is the capacitance, C_0 is the capacitance without the dielectric and δ is the angle by which current leads the voltage. Nitrobenzene, aniline and water were confined in ACF's, of pore width H = 1.7 nm at 1 atm. pressure. The complex dielectric permittivity $\kappa^* = \kappa' - i\kappa''$, was measured as a function of temperature and frequency.

For an isolated dipole rotating under an oscillating electric field in a viscous medium, the Debye dispersion relation is derived using classical mechanics,

$$\kappa^* = \kappa'_\infty + \frac{\kappa'_s - \kappa'_\infty}{1 + i\omega\tau} \tag{3}$$

In equation (3), ω is the frequency of the applied potential and τ is the orientational (rotational) relaxation time of a dipolar molecule. The subscript s refers to static permittivity (low frequency limit, when the dipoles have sufficient time to be in phase with the applied field). The subscript ∞ refers to the optical permittivity (high frequency limit) and is a measure of the induced component of the permittivity. The dielectric constant is a natural choice of order parameter to study freezing of dipolar liquids, because of the large change in the orientational polarizability between the liquid and solid phases. The dielectric relaxation time was calculated by fitting the dispersion spectrum of the complex permittivity near resonance to the Debye model of orientational relaxation.

Molecular simulation. We performed Grand Canonical Monte Carlo (GCMC) simulations of Lennard-Jones fluids adsorbed in regular slit shaped pores of pore width H and varying fluid-wall strengths. Here, H is the distance separating the planes through the centers of the surface-layer atoms on opposing pore walls. The interaction between the adsorbed fluid molecules is modeled using the Lennard-Jones (12,6) potential with size and energy parameters chosen to describe methane and CCl_4 [8,14]. The fluid-wall interaction is modeled using a "10-4-3" Steele potential [15],

$$\phi_{fw}(z) = 2\pi\rho_w\varepsilon_{fw}\sigma_{fw}^2\Delta\left[\frac{2}{5}\left(\frac{\sigma_{fw}}{z}\right)^{10} - \left(\frac{\sigma_{fw}}{z}\right)^4 - \left(\frac{\sigma_{fw}^4}{3\Delta(z + 0.61\Delta)^3}\right)\right] \tag{4}$$

Here, the σ's and ε's are the size and energy parameters in the LJ potential, the subscripts f and w denote fluid and wall respectively, and z is the coordinate perpendicular to the pore walls. The fluid-wall interaction energy parameters corresponding to a graphite pore were taken from [15]. For a given pore width H, the total potential energy from both walls is given by,

$$\phi_{pore}(z) = \phi_{fw}(z) + \phi_{fw}(H - z) \tag{5}$$

The strength of the fluid wall interaction is determined by the parameter $\alpha = \rho_w\varepsilon_{fw}\sigma_{fw}^2\Delta/\varepsilon_{ff}$. For example, in the case of methane, $\alpha = 0$ corresponds to a purely repulsive or hard wall, $\alpha = 0.76$ corresponds to a weakly attractive wall and $\alpha = 2.0$ corresponds to a strongly attractive graphite wall.

The simulation runs were performed in the grand canonical ensemble, fixing the chemical potential μ, the volume V of the pore and the temperature T. A pore width of $H = 3\sigma_{ff}$ was chosen to enable comparison with our experimental results. The system consisted of 600–12000 adsorbed molecules, depending on system size. For the case of attractive pore-wall interactions, the adsorbed molecules formed distinct layers parallel to the plane of the pore walls. A rectilinear simulation cell of dimensions L × L (where L was varied between $10\sigma_{ff}$ and $60\sigma_{ff}$) in the plane parallel to the pore walls was used. The simulation was set up such that insertion, deletion and displacement moves were attempted with equal probability, and the displacement step was adjusted to have a 50% probability of acceptance. Thermodynamic properties were averaged over 100–2000 million individual Monte Carlo steps. The length of the simulation was adjusted such that a minimum of fifty times the average number of particles in the system would be inserted and deleted during a single simulation run.

Free energy method. The method relies on the calculation of the Landau free energy as a function of an effective bond orientational order parameter Φ, using GCMC simulations [8]. The Landau free energy Λ is defined by,

$$\Lambda[\Phi] = -k_B T\ln(P[\Phi]) + constant \tag{6}$$

where $P[\Phi]$ is the probability density of observing the system having an order parameter value between Φ and $\Phi + \delta\Phi$, and k_B is Boltzmann's constant. The probability distribution function $P[\Phi]$ is calculated in a GCMC simulation as a histogram, with the help of umbrella sampling. The grand free energy Ω is then related to the Landau free energy by

$$\exp(-\beta\Omega) = \int d\,\Phi \exp(-\beta\Lambda[\,\Phi]) \qquad (7)$$

The grand free energy at a particular temperature can be calculated by numerically integrating equation (7) over the order parameter space. We use a two-dimensional order parameter to characterize the order in each of the molecular layers,

$$\Phi_j = \left| \frac{1}{N_b} \sum_{k=1}^{N_b} \exp(i6\theta_k) \right| = \left| \left\langle \exp(i6\theta_k) \right\rangle_j \right| \qquad (8)$$

Φ_j measures the hexagonal bond order within each layer j. Each nearest neighbor bond has a particular orientation in the plane of the given layer, and is described by the polar coordinate θ. The index k runs over the total number of nearest neighbor bonds, N_b, in layer j. The overall order parameter Φ is an average of the hexagonal order in all the layers. We expect $\Phi_j = 0$ when layer j has the structure of a two-dimensional liquid, $\Phi_j = 1$ in the crystal phase and $0 < \Phi_j < 1$ in an orientationally ordered layer.

RESULTS AND DISCUSSION

DSC and Dielectric Spectroscopy: DSC scans corresponding to melting of nitrobenzene, aniline and benzene confined in ACF are shown in Figure 1. In Figure 1 (a), the large peak at 5.6°C corresponds to the melting of the bulk nitrobenzene in
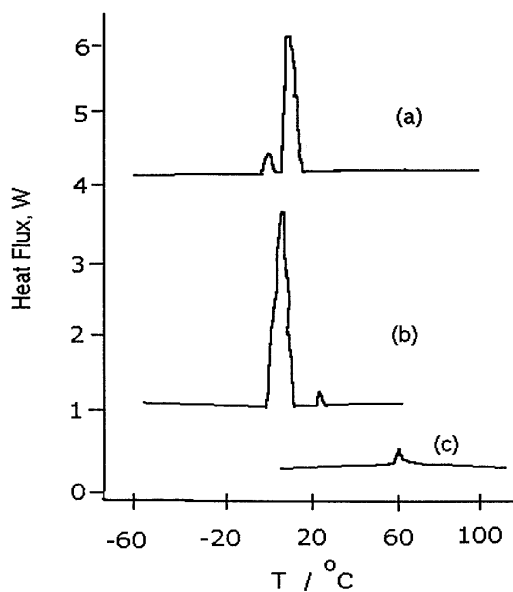

Figure 1. DSC scans for (a) nitrobenzene in ACF, (b) aniline in ACF, and (c) benzene in ACF, obtained as the systems were heated, starting from a low temperature.

which the ACF fibers are suspended. In addition, a second peak at 4.0°C is also observed, which corresponds to the melting of nitrobenzene in the pores of ACF; T_m is shifted to lower temperature due to confinement. In Figure 1(b), a large peak (corresponding to melting of bulk aniline) is observed at –5.0°C, while the melting of the confined aniline phase occurs at an elevated temperature of 25°C. For the case of benzene (Figure 1 (c)), the elevation in the melting temperature of the confined phase is even more dramatic, about 59°C; the bulk phase peak (at 6°C) is absent as benzene was adsorbed under saturated pressure; hence the suspension contained no excess bulk fluid.

The capacitance C and tangent loss $\tan(\delta)$ were measured as a function of frequency and temperature for nitrobenzene and aniline adsorbed in ACF. The orientational relaxation time, τ, was obtained by fitting $\kappa'(\omega)$ and $\kappa''(\omega)$ to the Debye equation (equation(3)). The behavior of the orientational relaxation time τ *vs. T* is shown in Figure 2. For nitrobenzene confined in ACF, there is a sharp decrease in the value of the relaxation time τ at $T = 0°C$, corresponding to the melting point of the confined fluid. The low temperature branch has a relaxation time of the order of 10^{-3} s, corresponding to the crystalline phase in the pores. The decrease in the value of τ by two orders of magnitude at 0°C corresponds to the melting of the confined crystal; the value of the melting temperature is consistent with the result from DSC in Figure 1 (a). The molecules in the confined liquid phase have a characteristic relaxation time of 5×10^{-6} s. This value is large compared to the relaxation time of the molecules in the bulk fluid. The measured relaxation time is that of the contact layers of nitrobenzene (adsorbed layers adjacent to the pore walls) that experience a deep potential energy well due to the pore walls, and hence are in a orientationally ordered hexatic state [16]. From Figure 2, the melting temperature for the confined crystalline phase of aniline is T = 30°C; this estimate is also consistent with the DSC scan in Figure 1(b).
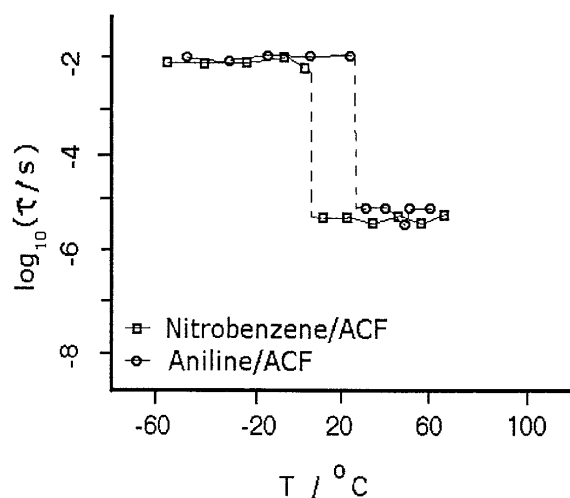

Figure 2. The orientational relaxation time τ (from DS experiments), of the molecules in the confined phase as a function of temperature for nitrobenzene and aniline confined in ACF.

Monte Carlo Simulation Results: Our goal is to further elucidate the importance of the strength of the fluid-wall interaction relative to the fluid-fluid interaction on the nature of the shift in the freezing temperature of fluids in confined systems. We performed molecular simulations and Landau free energy calculations for a LJ fluid confined in a slit shaped pore of width $H = 3\sigma_{ff}$, of varying fluid-wall interaction strengths. The value of α (see Experimental) was varied from $\alpha = 0.85$ to $\alpha = 2.2$ to model a range of pore wall potentials, ranging from weakly attractive to strongly attractive.

The Landau free energy calculations showed that for systems with a value of $\alpha < 0.9$, *i.e.*, for a fluid confined in a weakly attractive pore, the freezing temperature in the confined phase is less than that of the bulk phase. The opposite is true for systems with $\alpha > 0.9$, *i.e.*, for a fluid confined in a strongly attractive pore. For the real systems we have studied, *viz.*, nitrobenzene, aniline, and benzene in ACF, we calculate the value of α using Lennard-Jones parameters derived from bulk gas data (see [16]). The freezing temperatures of the confined phase expressed as $T_{m,pore}/T_{m,bulk}$ for values of α for these systems are shown in Table 1.

We have calculated the freezing temperatures in the confined phase as a function of the relative strengths of the fluid-wall and the fluid-fluid interaction, α. Following Radhakrishnan *et al*. [16], we can use the theory of corresponding states to show that the reduced freezing temperature of a LJ fluid in our model slit pore is largely determined by the values of α and *H*. We can use this powerful result to interpret our experimental findings. A comparison of the freezing temperatures (expressed as $T_{m,pore}/T_{m,bulk}$) obtained from our simulations with the experimental results is provided in Table l.

The close agreement between the results of our simulations and experiment is remarkable. It is worthwhile to note that in this work we are able to tune the value of α by varying the dipole moment of the fluid molecule. By varying the functional group of the benzene derivative, we vary the dipole moment, (benzene has zero dipole moment, aniline has a dipole moment of $\mu = 1.13$ D, nitrobenzene has a dipole moment of $\mu = 4.2$ D). The fluid-fluid interaction is strongly dependent on the dispersive as well as the dipolar components. However, owing to the small polarizability of the pore walls of ACF (the pore walls are composed of graphite), the fluid-wall interaction depends primarily on the dispersive component of the fluid molecules. Therefore, when confined in ACF, the fluid molecules with greater dipole moment experience a stronger fluid-fluid interaction compared to those with smaller dipole moment, while the fluid-wall interaction is little affected, leading to a reduction in α as the dipole moment increases. This is the reason why there is a lowering of freezing temperature for nitrobenzene confined in ACF ($\alpha = 0.85$), while benzene confined in ACF shows an elevation in the freezing temperature ($\alpha = 2.2$).

Table 1. Comparison of freezing temperatures in the confined phase obtained from simulation and experiment.

System	α (from ref. [16])	$T_{m,pore}/T_{m,bulk}$ (experiment)	$T_{m,pore}/T_{m,bulk}$ (simulation)
Nitrobenzene/ACF	0.85	0.98	0.97
Aniline/ACF	1.4	1.14	1.10
Benzene/ACF	2.2	1.23	1.25

Following this trend, we would expect a large decrease in the melting temperature of water confined in ACF. Although water has a permanent dipole moment of $\mu = 1.8$ D, the dispersive component of the fluid-fluid interaction is very small, and much smaller than the electrostatic component. Nevertheless, the total fluid-fluid attraction is very strong for water, because of the strong H-bonding interaction. Conversely, the fluid-wall interaction is primarily due to dispersion forces, which are very weak. As a consequence the value of α for the water/ACF system is 0.45, which is much lower than that of the nitrobenzene/ACF system. We therefore expect a large *decrease* in T_m for water in ACF. The DSC result for water in ACF in Figure 3 confirms this prediction. The melting temperature of the confined water phase (estimated from the position of the smaller peak in Figure 3) is $t = -40°C$. The value of $T_{m,pore}/T_{m,bulk} = 0.89$ for H_2O/ACF, which is smaller than the value for the nitrobenzene/ACF system, as expected.
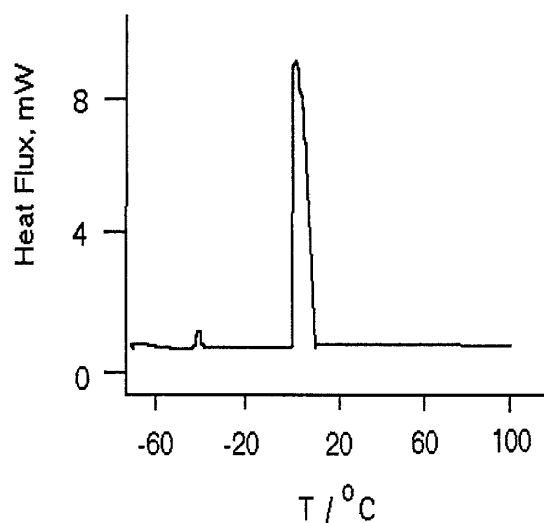
Figure 3. DSC scan for water in ACF, obtained as the system was heated, starting from a low temperature.

In future work we plan to develop global phase diagrams from simulation and experiment, to summarize the diverse freezing behavior of different fluids in different porous materials; this work is in progress and will be published elsewhere [20]. Efforts are also underway to use more realistic fluid potentials and pore models in the

simulation [21,22). These more realistic pore models include networking and poly-dispersity effects, and reproduce the structures of the real porous material very closely.

REFERENCES

1. Unger K.K., Kreysa G. and Baselt J.P., eds., *Characterisation of Porous Solids V*, Proceedings of the 5th international symposium on the characterization of porous solids, (Elsevier, Amsterdam), (2000).
2. Carbon '99, Proceedings of the 24th biennial conference on carbon, (American Carbon Society), (1999).
3. Warnock J., Awschalom D.D. and Shafer M.W., *Phys. Rev. Lett*., **57**(14),1753 (1986).
4. Unruh K.M., Huber T.E. and Huber C.A., *Phys. Rev. B*, **48**(12), 9021 (1993).
5. Sliwinska-Bartkowiak M., Gras J., Sikorski R., Radhakrishnan R., Gelb L.D. and Gubbins K.E., *Langmuir*, **15**, 6060 (1999).
6. Miyahara M. and Gubbins K.E., *J. Chem. Phys*., **106**(7), 2865 (1997).
7. Dominguez H., Allen M.P. and Evans R., *Mol. Phys*., **96**, 209 (1999).
8. Radhakrishnan R. and Gubbins K.E., *Mol. Phys*., **96**, 1249 (1999).
9. Klein J. and Kumacheva K., *Science*, **269**, 816 (1995).
10. Hu H.W., Carson G.A. and Granick S., *Phys. Rev. Lett*., **66**, 2758 (1991).
11. Granick S., *Science*, **253**, 1374 (1991).
12. Castro M.A., Clarke S.M., Inaba A. and Thomas R.K., *J. Phys. Chem*., **101B**, 10528 (1998).
13. Christenson H.K., *Colloids Surf. A*, **123**, 355 (1997).
14. Radhakrishnan R., Gubbins K.E., Watanabe A. and Kaneko K., *J. Chem. Phys*., **111** (19), 9058 (1999).
15. Steele W.A., *Surf Sci*., **36**, 317 (1973).
16. Radhakrishnan R., Gubbins K.E., Sliwinska-Bartkowiak M., *J. Chem. Phys*., **112**(24), 11048 (2000).
17. Watanabe A., Iiyama T., Kaneko K., Radhakrishnan R. and Gubbins K.E., *J. Phys. Chem*., **103**(34), 7061 (1999).
18. Maddox M.W. and Gubbins K.E., *J. Chem. Phys*., **107**, 9659 (1997).
19. Radhakrishnan R., Gubbins K.E., Sliwinska-Bartkowiak M., Dudziak G., Sikorski, R. and Gras R., *J. Chem. Phys*., in press (2000).
20. Radhakrishnan R., Gubbins K.E. and Sliwinska-Bartkowiak M., to be published.
21. Gelb L.D. and Gubbins K.E., *Langmuir*, **14**, 2097 (1998).
22. Thomson K.T. and Gubbins K.E., *Langmuir*, **16**, 5761-5774 (2000).